

# CFD ANALYSIS OF PRESSURE DROPS WITHIN RIFFLED PIPES OF VERTICAL GROUND HEAT EXCHANGER

ANDRZEJ J. NOWAK<sup>1</sup>, JACEK SMOLKA<sup>1</sup>, MICHAL PALACZ<sup>1</sup>,  
MICHAL HAIDA<sup>1</sup> AND JEREMI WOS<sup>2</sup>

<sup>1</sup> Silesian University of Technology  
44-100 Gliwice, Konarskiego 22, Poland  
andrzej.j.nowak@polsl.pl and www.itc.polsl.pl/nowak

<sup>2</sup> "ELPLAST+"  
44-336 Jastrzebie-Zdroj, Niepodleglosci 8, Poland  
jeremi.wos@elplastplus.pl and <https://elplastplus.pl/>

**Key words:** Pressure Drops, Vertical Ground Heat Exchanger, Riffled Pipe, Micro-Fins, Effect of Deformation

**Abstract.** In this work 3D CFD analysis of a fluid flow problem within vertical ground heat exchanger is discussed. Both downward and upward pipes of the heat exchanger are made of polyethylene (PE100) and they are equipped with internal micro-fins. These fins form a sort of threads with the pitch varying between 1200 mm and 1600 mm. Both pipes (almost 250 meter long each) are connected at the lowest point either by standard U-turn or by specially designed bottom chamber. Two different water-ethanol solutions circulate within the pipes of the heat exchanger.

Because of the heat exchanger length the whole computational domain was divided into three parts: inlet part, reversal or both pipes connection and remaining pipes for which pressure drops depend linearly on the pipe length. These three parts were analysed separately and obtained solutions have finally been coupled iteratively.

## 1 INTRODUCTION

Ground is an attractive source of heat and one of the most popular way of extracting heat from the ground is the application of a vertical ground heat exchangers. Such heat exchanger consists generally of two vertical pipes, i.e. downward and upward ones, connected by the reversal as shown schematically in Fig. 1. Typically they are classified as either closed loops or open loops depending on how they utilise the fluid flowing through the system. Overview of the most frequently used models and systems can be found elsewhere, for instance in [1]. No matter which solution is considered, the operating costs of the heat exchanger (and in consequence of the whole installation) depends strongly on the pumping power which is proportional to the total pressure drop of the installation, the volume flow rate of the working fluid and energy efficiency of the pumps. From these three parameters the first one, i.e. the total pressure drop is the most difficult to be

determined. This task is particularly challenging if pipes of the ground heat exchanger are equipped with some internal fins or installation contains reverse or bottom chamber of special design. Example of such application can be found for instance in [2].

The main aim of this work is to propose a numerical procedure to determine the pressure drop within the ground heat exchanger, including pressure drops caused by classical U-turn but also special bottom chamber. The heat exchanger is built of the internally finned pipe, or more precisely riffled pipe. The riffled pipe (its cross-section is shown in Fig. 2) is frequently applied in Scandinavia to build vertical-borehole ground-coupled heat pumps.

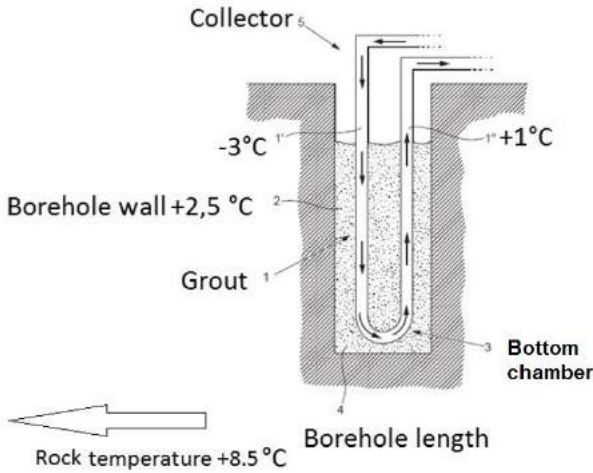


**Figure 1:** Sketch of the vertical ground heat exchanger.

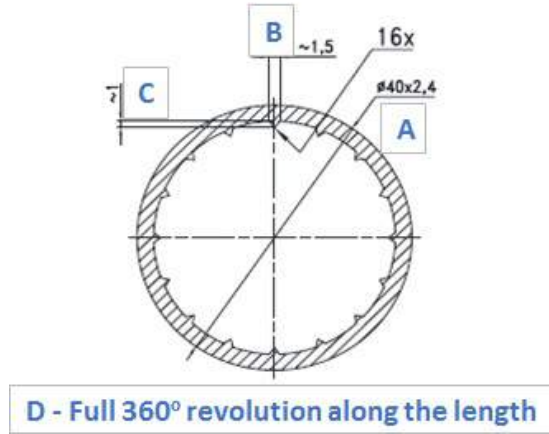


**Figure 2:** Cross-section of the riffled pipe.

The next section of this work presents details of the solution methodology including governing equations, adopted turbulence model and boundary conditions. All geometrical data as well as material and transport properties of working fluid required to perform all computations are collected in Section 3. In Section 4, selected numerical results obtained using Ansys/Fluent package are presented and discussed together with dimensionless equation allowing one to estimate a total pressure drops in ground heat exchanger. Concluding remarks are formulated at the end of the paper.

## 2 COMPUTATIONAL MODEL OF THE SOLUTION FLOW WITHIN RIFFLED PIPE AND BOTTOM CHAMBER

### 2.1 General approach and flow equations

The ground heat exchanger considered in this work is made of polyethylene PE100 riffled pipe [3]. The Standard Dimension Ratio (SDR) of this pipe is 17. The pipe has 16 small triangle internal fins (their height is roughly 1 mm) placed symmetrically along the pipe circuit as it is shown in Fig. 2. The fins form a sort of threads with the pitch varying between 1200 mm and 1600 mm.

The heat exchanger consists generally of two vertical pipes, i.e. downward and upward ones, connected by the U-turn either made of two 90° elbows called U-turn A in this work

and shown in Fig. 4, or having a form of the bottom chamber called U-turn B in this work and shown in Fig. 5. It should be noted that pipes being a part of the U-turns do not have any fins.

In typical working conditions temperature changes of the heat transfer carrier (water-ethanol solution) are generally small. Therefore, in the analysis performed here, it is assumed that the average temperature of the fluid is equal to +1°C and can be treated as constant. It is also assumed that the concentration of the water-ethanol solution is either 24% or 35%.

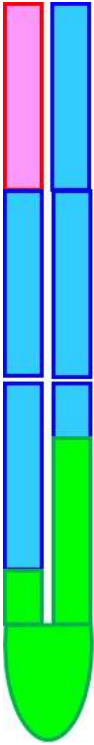


**Figure 3:** Three basic parts of the heat exchanger.

The borehole length can be even as long as 250 meters therefore numerical discretisation of vertical pipes of the ground heat exchanger would result in a huge number of volume cells certainly exceeding the capacity of modern computer memory and acceptable computing time. Therefore, modelling water-ethanol solution flow, the whole collector has been divided into following three basic parts shown schematically in Fig. 3:

- entrance distance of the downward pipe having length bigger than 50 diameters of the pipe. This part is marked by magenta colour in Fig. 3,
- U-turn with the long enough outflow (upward) pipe. Its length should again be bigger than 50 diameters of the pipe. This part is marked by green colour in Fig. 3,
- long downward pipe as well as long upward pipe (marked by blue colour in Fig. 3) in which pressure drops depend linearly on the pipe length. The pressure drop along 1 meter of the pipe was determined modelling solution flow within repeatable segment of the pipe having the length equal to the pitch of the thread. The pipe with the thread pitch of 1200 mm is denoted as Pipe A, while the rifflled pipe with the thread pitch of 1600 mm is denoted as Pipe B.

Modelling of the flow field within repeatable segment of the pipe, one has to determine both inlet and outlet velocity fields. This requires iterative calculations in which outflow field obtained in the current iteration is prescribed as the inlet flow field in the next iteration. That iterative loop is terminated if difference between two successive flow fields is smaller than acceptable calculation accuracy.

The framework for the development of the above discussed steady-state flow models is based on standard balances of mass and momentum [4, 5], i.e. continuity and Navier-Stokes equations which for a Newtonian fluid can be written as:

$$\nabla \cdot (\rho \cdot \mathbf{v}) = 0 \tag{1}$$

$$\varrho \cdot (\mathbf{v} \cdot \nabla) \mathbf{v} = \varrho \cdot \mathbf{g} - \nabla p + (\mu + \mu_t) \cdot \nabla^2 \mathbf{v} \quad (2)$$

where  $\mathbf{v}$  denotes the velocity vector that (in general) is a function of time and position (i.e. geometrical coordinates). The fluid density is represented by  $\varrho$ ,  $\mu$  and  $\mu_t$  stand for the fluid dynamic viscosity and turbulent viscosity, respectively. The term  $\nabla p$  represents the gradient of the static pressure and  $\mathbf{g}$  is the gravitational acceleration vector. Equations (1) and (2) need to be solved using Ansys/Fluent commercial CFD software [6].

## 2.2 Adopted turbulence model

It is commonly accepted that the working fluid nominal flow that occurs in the riffled pipe should be around beginning of turbulent regime and relevant Reynolds numbers are generally fairly low. Therefore, the turbulence model eventually adopted in this work was  $k - \omega$  model utilising the turbulence kinetic energy,  $k$ , and the specific dissipation rate,  $\omega$ . These two quantities can be obtained from the transport equations proposed either by standard  $k - \omega$  or share-stress transport (SST)  $k - \omega$ . The details of both models can be found for instance in [6] and [7]. It should be emphasised that in fact both  $k - \omega$  models produce very similar results. Turbulent viscosity  $\mu_t$  is then obtained from the following relationship:

$$\mu_t = \varrho \frac{k}{\omega} \quad (3)$$

and substituted to Equation (2). It should also be stressed that in this work, the turbulence intensity is additionally used to identify a degree of the flow turbulence. This problem will be discussed in Section 4.

## 2.3 Prescribed boundary conditions

In all three basic parts of the collector considered in this work, a standard no slip boundary condition was prescribed on all physical walls. For the entrance distance of the downward pipe marked by magenta colour in Fig. 3, uniform inlet velocity was assumed, while the outlet velocity profile has been obtained as a result of the numerical modelling.

The inlet velocity profile for U-turn A or B (marked by green colour in Fig. 3) was determined analysing the flow of the water-ethanol solution through the repeatable segment of the pipe marked by blue colour in Fig. 3.

As already mentioned, modelling of flow field within repeatable segment of the pipe requires iterative calculations in which the outflow field obtained in the current iteration is prescribed as the inlet flow field in the next iteration.

## 2.4 Determination of pressure drop

Solving system of Equations (1) and (2), one obtains the information about many physical fields including the pressure field. A result related to the repeatable segment of the riffled pipe needs to be multiplied by the length of the pipe in which pressure drop is linear to get a total pressure drop within that pipe. Summing up that result with the

local pressure drops for entrance distance and U-turn, one obtains the total pressure drop for the whole heat exchanger.

### 3 MODEL INPUTS

#### 3.1 Geometrical data and transport properties of the solutions

The main geometrical data characterising riffled pipe and U-turns are given in Figs. 2, 4 and 5 together with Tables 1 and 2.

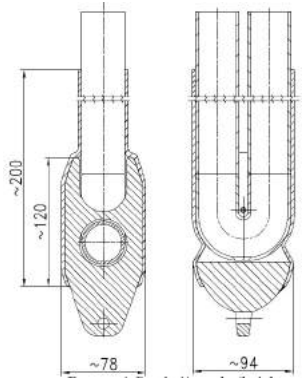


Figure 4: Cross-section of the U-turn A.

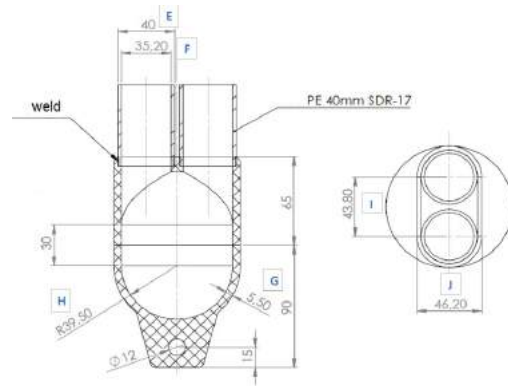


Figure 5: Cross-section of the U-turn B.

Table 1: The main geometrical data of the riffled pipe.

Pipes PE-100				
Dimension	Par. Name	Unit	Value	
Inner pipe diameter	A1	m	0.0352	
Wall thickness	A2	m	0.0024	
Single rib width	B	m	0.0015	
Single rib height	C	m	0.0015	
Full 360° inner pipe revolution along pipe axis	D	m	1.2	1.6

Table 2: The main geometrical data of U-turn B.

Bottom chamber				
Dimension	Par. Name	Unit	Value	
Outer pipe diameter	E	m	0.04	
Inner pipe diameter	F	m	0.0352	
Bottom chamber thickness	G	m	0.0055	
Bottom chamber radius	H	°	39.5	
Distance between the pipes axis	I	m	0.0438	
Outer width of the pipe inlet	J	m	0.0462	

The main thermal and transport properties of the 24% and 35% water-ethanol solutions [8] are collected in Tables 3.

**Table 3:** The main thermal and transport properties of the 24% and 35% water-ethanol solutions.

#1 Water - Ethanol Concentration : 0.24			#2 Water - Ethanol Concentration : 0.35		
Properties	Unit	Value	Properties	Unit	Value
Temperature	oC	1.00	Temperature	oC	1.00
Density	kg/m3	972.00	Density	kg/m3	957.40
Specific heat	kJ/(kg K)	4.292	Specific heat	kJ/(kg K)	4.051
Conductivity	W/(m K)	0.4285	Conductivity	W/(m K)	0.375
Dynamic viscosity	Pa s	0.005484	Dynamic viscosity	Pa s	0.006515
Kinematic viscosity	m <sup>2</sup> /s	5.64E-06	Kinematic viscosity	m <sup>2</sup> /s	6.80E-06

### 3.2 Numerical mesh

As already mentioned in Section 1, the generated numerical mesh needs to be fine enough to guarantee the mesh-independent results of computer simulations. In addition, dimensions of numerical cells neighbouring to the pipe wall have to be appropriate to represent well so-called boundary layer.

Taking into account above constrains, the numerical mesh created for fluid flowing within riffled pipe is very dense in the vicinity of fins and is twisted along threads lines. This is demonstrated in Fig. 6. Fig. 7 presents the details of the mesh cross-section that is perpendicular to the pipe axis. The mesh for Pipe A (the thread pitch of 1200 mm) consists of almost 10 mln elements, while similar mesh for Pipe B (the thread pitch of 1600 mm) contains 15 mln of cells.

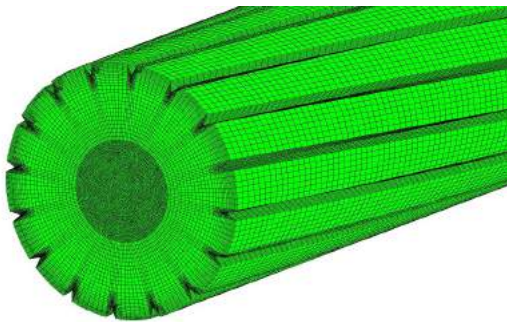


**Figure 6:** Numerical mesh for fluid in the riffled pipe.

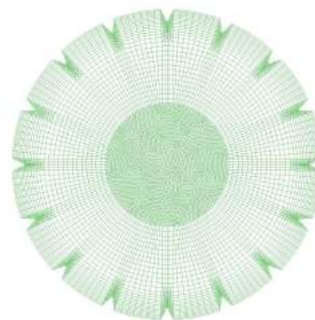


**Figure 7:** Cross-section of the numerical mesh for fluid in the riffled pipe.

The numerical mesh for U-turn A made of two 90° elbows was generated in a very similar way. It consists of 130 thous. of volume cells and is shown in Fig. 8 and 9. The upward pipe (right one) is longer to determine fully developed outflow field.

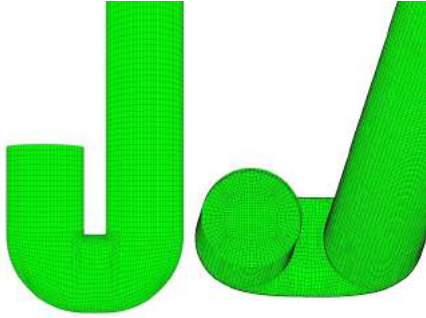


**Figure 8:** Numerical mesh for fluid in U-turn A having a form of the standard two elbows.

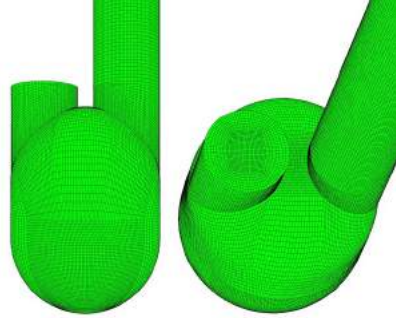


**Figure 9:** Numerical mesh for fluid in U-turn B having a form of the bottom chamber.

#### 4 SELECTED RESULTS AND THEIR DISCUSSION

Although as mentioned in Section 2, the computations were performed for two compositions of the working fluid, i.e. the 24% and 35% water-ethanol solution flowing through the considered vertical ground heat exchanger, mainly results for the the first concentration are presented here due to limited space. The results are presented along two diameters of Pipe A (1200 mm for a full thread revolution) and Pipe B (1600 mm for a full thread revolution). The location of those diameters is presented in Fig. 10. In this figure, the diameters denoted as Diameter 1 and Diameter 2 connect the fin tips (continuous line) and the internal walls between fins (dotted line), respectively. In addition, the local pressure loss determined for the U-turns is discussed. These parts are referred to as U-turn A for the two 90° elbows shown in Fig. 4 and U-turn B for the bottom chamber shown in Fig. 5.

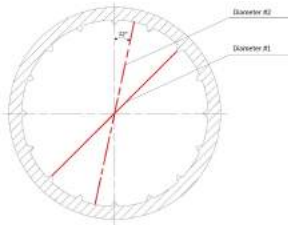


**Figure 10:** Diameter position for the results presentation along the pipe diameter in Section 4.

The considered flow cases cover six values of the Reynolds number of 2750 (on-design case), 2110, 1700, 1500, 1200 and 1000 for the concentration of the 24% water-ethanol solution and the Reynolds number of 2300 (on-design case), 1750, 1400, 1200, 1000 and 800 for the concentration of the 35% water-ethanol solution.

Figs. 11-16 present axial, radial and tangential velocities along Diameter 1 and 2 for all the considered flow cases in Pipe A and B, respectively. When the velocity profiles in these figures are compared, it becomes clear that the axial velocity dominates over the two remaining velocity vector components in the flow core. In particular, the axial velocity is by two order of magnitude larger than the radial and tangential velocities. The situation drastically change in the near wall layer. In this region, the axial velocity component is substantially reduced. This also means that the other velocity components play a more important role resulting in the swirl flow.

Another observation is related to the shape of the axial velocity profile presented in Figs. 11 and 12. For higher Re numbers, the steeper axial velocity profile near the walls

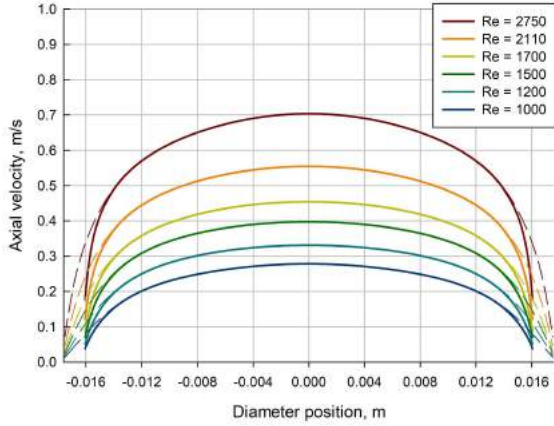


**Figure 11:** Axial velocity in m/s along the pipe diameter for all the considered cases in Pipe A.

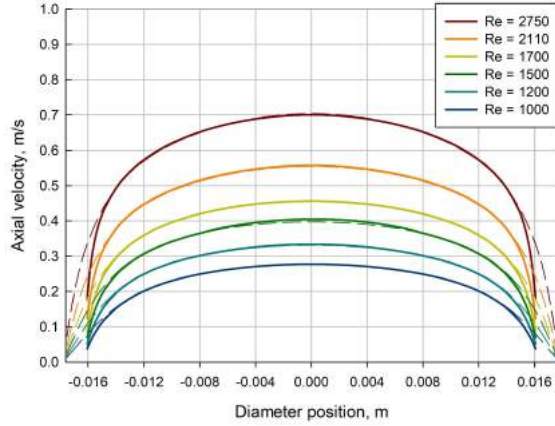


**Figure 12:** Axial velocity in m/s along the pipe diameter for all the considered cases in Pipe B.

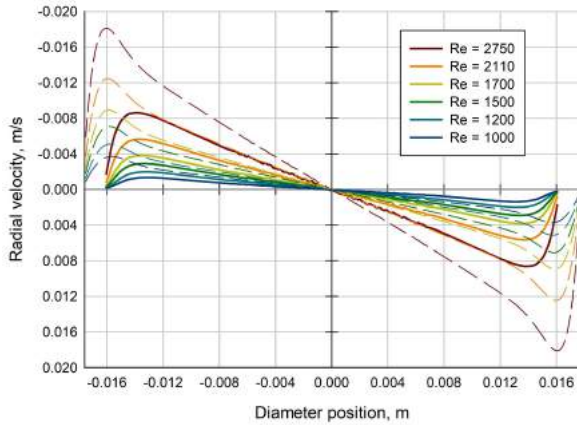


**Figure 13:** Radial velocity in m/s along the pipe diameter for all the considered cases in Pipe A.

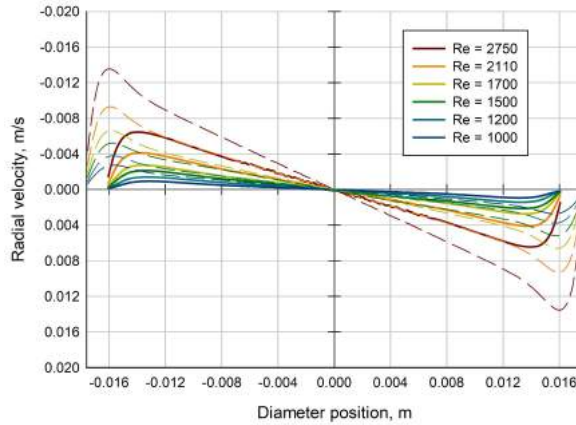


**Figure 14:** Radial velocity in m/s along the pipe diameter for all the considered cases in Pipe B.

occurred in both pipe types. In contrary, the results obtained for low Re numbers showed a more flat profile. These profile shapes are consistent with the theory.

In Figs. 17 and 18, the turbulence intensity along both pipe diameters of Pipe A and B is presented, respectively. For both pipe types, the turbulence intensity profile was of the saddle shape. This means that the parameter has a noticeable lower value in the pipe axis than in the region of the pipe fins.

Another observation that can be made is the shape of the turbulence intensity profile for the low and high Re numbers. It can clearly be seen that the profile saddle shape is much more flat for low Re flow when compared with the high Re flow.

The computed pressure drop in Pipe A and B per each meter of the pipe length is presented in Figs. 19 and 20. As shown in both figures, the pressure drop is almost identical for both pipes. It should also be noted that the pressure drop is constant within

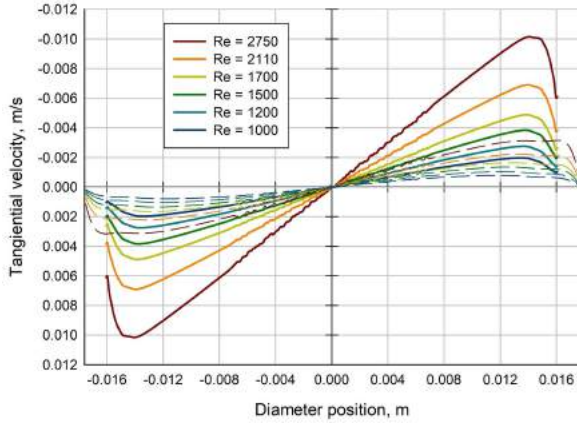


**Figure 15:** Tangential velocity in m/s along the pipe diameter for all the considered cases in Pipe A.

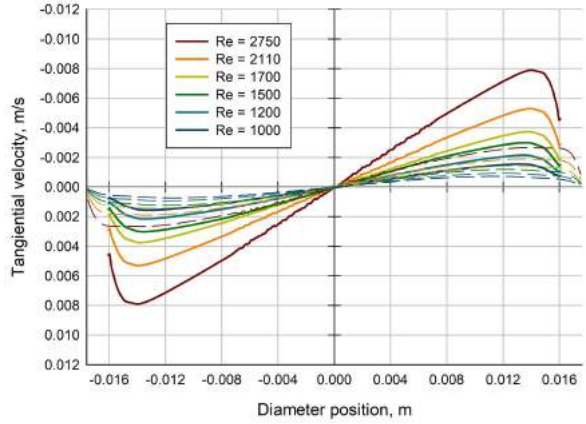


**Figure 16:** Tangential velocity in m/s along the pipe diameter for all the considered cases in Pipe B.

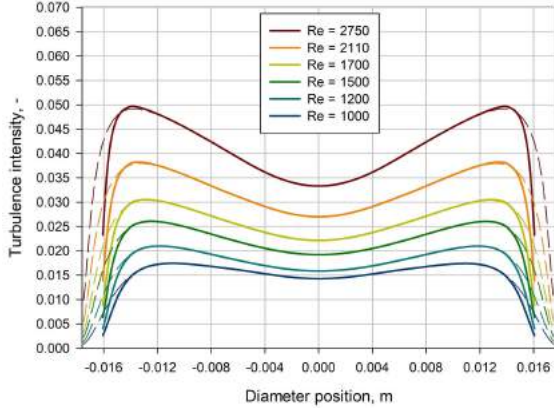


**Figure 17:** Turbulence intensity along the pipe diameter for all the considered cases in Pipe A.

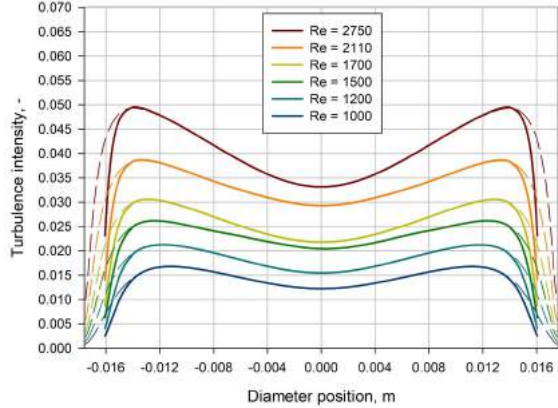


**Figure 18:** Turbulence intensity along the pipe diameter for all the considered cases in Pipe B.

both pipes at the given Re number. The linear behaviour of the pressure loss in the considered pipes is consistent with the theory and the pressure loss in Pa/m can be approximated by the following formula (with  $R$  squared above 0.999):

$$\Delta p = 14.677 \left( \frac{Re}{1000} \right)^2 + 35.309 \left( \frac{Re}{1000} \right) - 12.812 \quad (4)$$

The local pressure drop caused by both U-turns occurred in the U-turn itself and the first part of the upward pipe. To distinguish those pressure losses, the pressure loss was separately presented in Figs. 21 and 22 for the local pressure loss in the U-turn A and B itself and in Figs. 23 and 24 for the first segment of the upward pipe after U-turn A and B.

These figures show that the local pressure loss is significantly larger in the U-turn itself

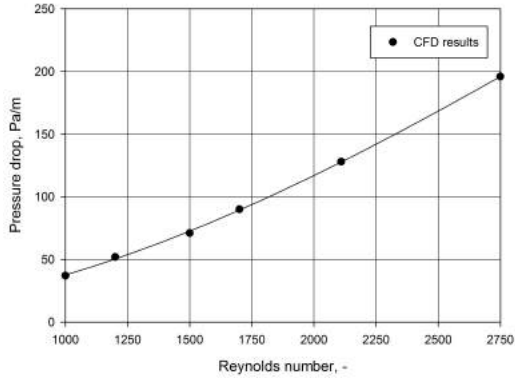


**Figure 19:** Pressure drop along 1 m of the pipe segment for all the considered cases in Pipe A.

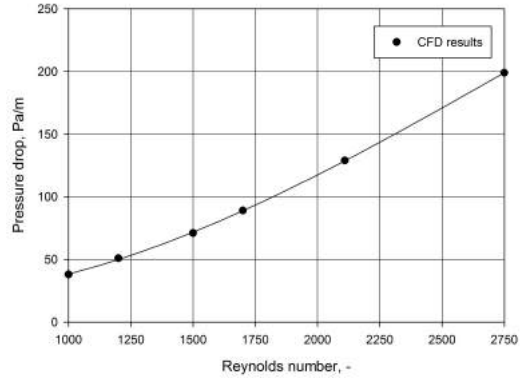


**Figure 20:** Pressure drop along 1 m of the pipe segment for all the considered cases in Pipe B.

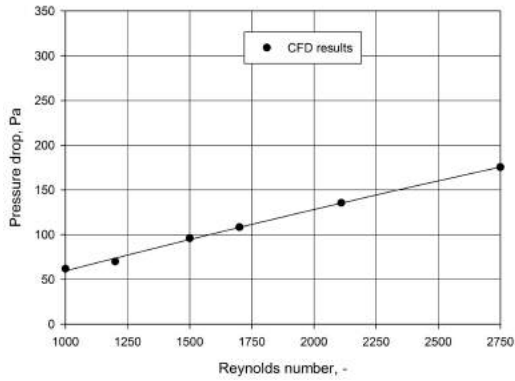


**Figure 21:** Local pressure drop in U-turn A for all the considered cases.

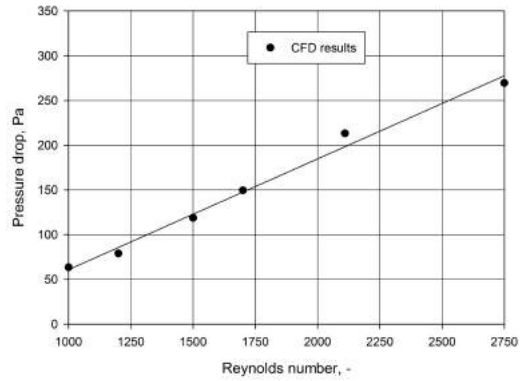


**Figure 22:** Local pressure drop for in U-turn B all the considered cases.

when compared to the other local loss. However, the local losses in the upward pipe are

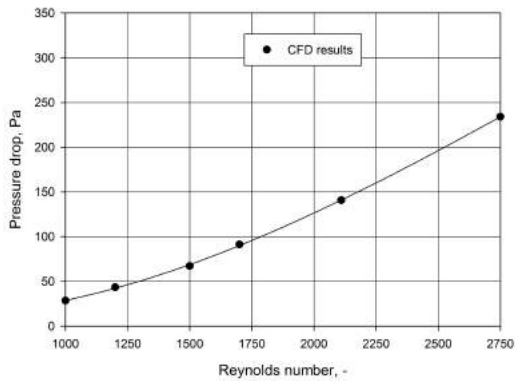


**Figure 23:** Local pressure drop in the pipe after U-turn A for all the considered cases.

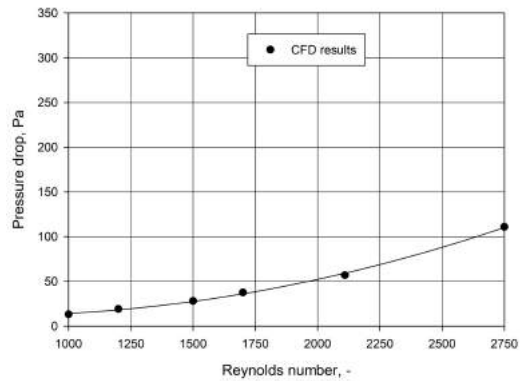


**Figure 24:** Local pressure drop in the pipe after U-turn B for all the considered cases.

noticeably larger for U-turn A and smaller for U-turn B when compared to the losses that occurred in the developed flow in a straight pipe segment of 1 m.

In Figs. 25 and 26, a sum of the local pressure loss for U-turn A and B, respectively is presented. These data are just summation of relevant data from Fig. 21 or Fig. 22 and data from Fig. 23 or 24.

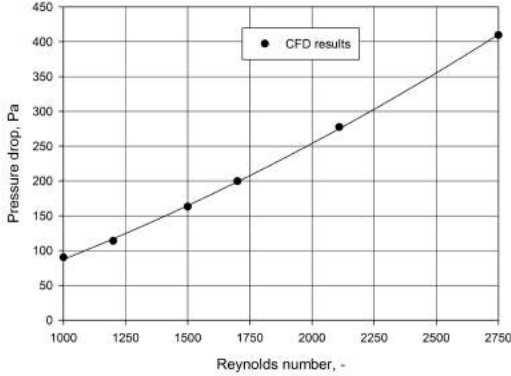


**Figure 25:** Sum of the local pressure drop for all the considered cases in U-turn A.

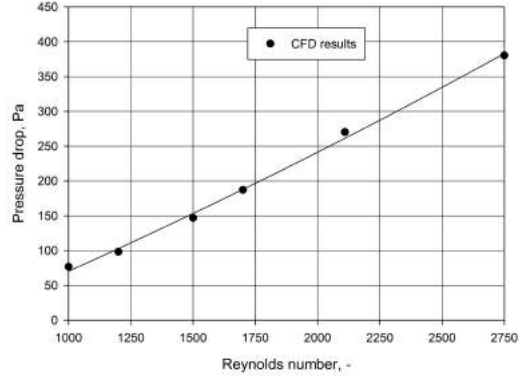


**Figure 26:** Sum of the local pressure drop for all the considered cases in U-turn B.

The total pressure drop in the vertical ground heat exchanger can be calculated by summing up the linear pressure drop presented in Figs. 19 and 20 for a particular length of Pipe A and Pipe B, respectively and the local pressure drop presented in Figs. 25 and 26 for U-turn A and U-turn B, respectively. For example, the vertical ground heat exchanger that consists of both downward and upward pipes of type Pipe A with the length of 200 m each and U-turn A working at the on-design conditions, i.e. the Re number of 2750, is characterised by the total pressure loss of 80.4 kPa.

Many computer simulations also proved that ovality of the pipe which may occur in transport, storing of pipes in coils, applying of clamping devise, etc. does not noticeably changing above results.

## 5 GENERAL CONCLUSIONS

On the basis of the performed CFD analysis, it can be said that computer modelling of the water-ethanol solutions flow within the vertical ground heat exchanger (collector) is a very challenging task mainly because of length of analysed object. In a consequence, the object had to be divided into three parts and then the obtained solutions have to be coupled. Presence of micro-fins within the rifflid pipe complicate considerably generation of the numerical mesh which requires a lot of attention.

The velocity field showed that the axial flow dominates over the radial and tangential flow in the flow core in both Pipe A and B. The flow character changes in the near wall region where the axial velocity is significantly reduced, while the radial and tangential velocities reach their maximum values. This means that near the boundary the flow is also swirled. As expected, the swirl flow is more intensive in Pipe A. However, these

differences are not large.

The turbulence intensity showed that for the flow with Re number above 2100, this parameter is higher by 1% in the near wall region than in the pipe axis. For lower Re numbers, this difference is much lower. These observations are the same for Pipe A and B.

The pressure drop obtained for the straight segments of Pipe A and B showed that these pressure losses are practically the same. In addition, the pressure loss decreases almost linearly with the decreasing Re number. The total pressure drop in the whole heat exchanger is mainly due to the losses that occur in the straight pipes. Even for shorter pipes, e.g. of 100 m in length, the local pressure loss in the U-turn is not important when compared to the total pressure loss.

In general, the observations of the results obtained for both water-ethanol concentrations are very similar qualitatively. However, it can be noticed that all type pressure losses for Concentration 2 are higher than that of Concentration 1 for the corresponding Re numbers.

## ACKNOWLEDGEMENT

The authors gratefully acknowledge the financial support of the Research Council of Norway through project No. 244009/E20.

## REFERENCES

- [1] Florides, G., Kalogirou S., Ground heat exchangers A review of systems, models and applications. *Renewable Energy*, **32**, (2007), 24612478.
- [2] Acuña J., Palm B., Experimental comparison of four borehole heat exchangers. *Refrigeration Science and Technology Proceedings*, Copenhagen: International Institute of Refrigeration, 2008, p. SEC09-W1-09.
- [3] Web address <https://elplastplus.pl/produkty/rury-do-geotermii/>
- [4] Patankar, S. V. *Numerical Heat Transfer and Fluid Flow*. Hemisphere Publication Corporation. New York; 1980.
- [5] Ferziger, J. H. and Peric M. *Computational Methods for Fluid Dynamics*. 3<sup>rd</sup> Edition; Springer. New York; 2002.
- [6] *Ansys Fluent 12.1 in Workbench Users Guide*, ANSYS, Inc. (2009).
- [7] D. C. Wilcox. *Turbulence Modeling for CFD*. DCW Industries, Inc., La Canada, California, 1998.
- [8] Bell, Ian H. and Wronski, Jorrit and Quoilin, Sylvain and Lemort, Vincent. Pure and Pseudo-pure Fluid Thermophysical Property Evaluation and the Open-Source Thermophysical Property Library CoolProp. *Industrial & Engineering Chemistry Research*, **53**, 6, pp 2498–2508, 2014.